POAC'25
St. John's, Newfoundland and Labrador, Canada

Proceedings of the 28th International Conference on Port and Ocean Engineering under Arctic Conditions
Jul 13-17, 2025
St. John's, Newfoundland and Labrador
Canada

Assessing the predicting capabilities of two turbulence models for flow simulation around the tip section of NREL 5MW offshore wind turbine blade

Emmanuel Quayson-Sackey [1], Saroj Gautam [2], Baafour Nyantekyi-Kwakye[1]
[1]Dalhousie University, Nova Scotia, Canada
[2] Memorial University of Newfoundland, St. John's, Newfoundland and Labrador

ABSTRACT

The accurate prediction of turbulent flow around a blade is critical for optimizing aerodynamic performance, particularly in applications such as offshore wind turbines (OWT). This study compares the predictive capabilities of Unsteady Reynolds-Averaged Navier-Stokes (URANS) and Detached Eddy Simulation (DES) for simulating the flow around the tip section of the NREL 5MW OWT blade. A scaled windward blade tip section which comprises of NACA 64-618 airfoils were used for this qualitative investigation, focusing on flow characteristics such as vortex shedding, flow separation, and the evolution of vortex structures, all of which are important in offshore wind energy applications. It was observed that URANS, which averages turbulent quantities, provides good predictions for attached flows but underpredicts separated flows, particularly at high angles of attack (α = 12°). In contrast, DES, a hybrid approach combining RANS in the near-wall region and LES in the wake offered a more accurate representation of unsteady turbulence, capturing detailed vortex structures, flow separation, and recirculation regions. The results show that DES significantly improves the prediction of turbulent flow and separation at the trailing edge, while URANS fails to resolve key unsteady flow phenomena.

KEY WORDS: Turbulence; Reynolds-averaged Navier-Stokes; Detached eddy simulation; Offshore wind energy.

INTRODUCTION

The accurate prediction of turbulent flow around airfoils is crucial for aerodynamic performance assessment in various engineering applications, including aircraft design, wind turbine ice mitigation, and turbomachinery (Hasheminasab et al., 2021; Quayson-Sackey et al., 2024). Computational Fluid Dynamics (CFD) methods provide a powerful tool for analyzing these flows, with URANS, DES, and Large Eddy Simulation (LES) being among the most commonly used turbulence modeling approaches. Each turbulence modeling approach presents distinct trade-offs in accuracy, computational demand, and applicability. The present research examines and compares the predicting capabilities of these three methods in terms of accuracy, computational cost, and applicability to different flow regimes around NACA64-618.

Turbulent flow around an airfoil is characterized by unsteadiness, variation in pressure gradient and flow separation that contribute to vortex formation and propagation. The URANS models the entire turbulence spectrum using Reynolds-averaged equations, incorporating time-dependent terms to capture unsteady phenomena. LES resolves large turbulence structures explicitly while modeling only the smallest eddies using a subgrid-scale model. The DES model is a hybrid approach that blends RANS near the wall with LES in separated flow regions,

offering a compromise between computational efficiency and turbulence resolution. Regardless of recent technological advances, URANS remains widely used for steady and mildly unsteady turbulent flows. Research have shown that URANS effectively predicts attached flows but faces major limitation with massively separated flows (Spalart, 2000, Menter, 1994, Rumsey & Gatski, 2001). It should also be noted that although RANS-based simulations provide reasonable accuracy at low angles of attacks, relatively very large discrepancies occur between numerical and experimental results at high angles of attacks, where flow separation is present.

Various research groups have explored the causes of inaccuracies at higher angles of attack, along with the effectiveness of different methods and models (Bangga et al., 2018a Xiao & She, 2020, Rumsey and Gatski, 2001). A thorough review on the performance of various RANS models in by Argyropoulos and Markatos (2015) concluded that the two-equation models yield more accurate results than the one-equation models, particularly when predicting separated flow. However, as demonstrated by Rumsey and Gatski (2001), majority of RANS models cannot reliably capture the region near maximum lift. Bangga et al. (2020) employed a modified URANS to investigate two-dimensional flow around four airfoils. To improve the predicting capability of their model, the authors adjusted the turbulent viscosity of the eddy-viscosity Menter Shear-Stress-Transport model. Their improved model adequately predicted the maximum lift coefficient, due to better capture of the separated region under intense pressure gradient and overestimated the stall angle. The observed discrepancies are in away expected due to three dimensionality and unsteadiness of the turbulent flow. Applying eddy-resolving models like LES or DES has been shown to improve the predictability of these aerodynamic measures (Bangga et al., 2018b).

Since coherent vortical structures dominate such turbulent flows, various vortex evolution techniques have been used to analyze turbulent flow around airfoils to provide insights into vortex shedding, flow separation, and reattachment phenomena. Techniques, such as, Q-criterion, λ_2 criterion, and swirling strength are used to isolate coherent vortex structures from the turbulent background flow (Chakraborty et al., 2005, Jeong & Hussain, 1995). Studies by Lee & Sung (2001) and Kato & Nagano (1993) have demonstrated the ability of using URANS to predict periodic vortex shedding in flows past bluff bodies and airfoils, though with limitations in fine-scale turbulence resolution. Although URANS can capture large-scale vortices, it lacks the resolution to fully characterize small-scale turbulence and vortex breakdown. The foregoing discussion suggests that although the URANS have been successfully applied in low-Reynolds-number flows, it fails in highly unsteady or massively separated conditions. To effectively capture large-scale motion, Wang et al. (2014), Mittal and Moin (1997), and Garnier et al. (2009) utilized LES to fully resolve flow separation, dynamic stall and vortex shedding within the wake region of an airfoil. These studies showed that the LES is particularly effective in resolving trailing-edge vortices and shedding phenomena, which are crucial for noise prediction and aerodynamic performance optimization.

Information from the literature shows that extensive research has been conducted to explore the predicting capabilities of different turbulent models on blades using URANS, LES and DES. However, their unsteady effects on an offshore wind turbine blade section have not been extensively investigated and fully understood as more complex flow phenomena such as flow separation, vortex shedding plays a role. Therefore, this study focuses on comparing the performance of two turbulence models, URANS and DES, for simulating the flow around the tip section of the NREL 5MW offshore wind turbine blade at a high angle of attack ($\alpha = 12°$). Although considered object of study has not been installed as a commercial OWT, it has over the years been considered as a standardized baseline for offshore wind research due to its widespread use in studies simulating offshore conditions.

NUMERICAL SETUP

Governing equations

The governing equations for turbulence modeling in this study are based on the URANS equations and DES equations. Incompressible viscous flow around the blade was simulated by the finite volume method to solve the Navier-Stokes equation. The governing equations for the mass and momentum conservation is written as;

$$\frac{\partial u_i}{\partial x_i} = 0 \tag{1}$$

$$\frac{\partial}{\partial t}(\rho u_i) + \frac{\partial}{\partial x_j}\left(\rho u_i u_j\right) = -\frac{\partial p}{\partial x_i} + \frac{\partial}{\partial x_j}\left[\mu\left(\frac{\partial u_i}{\partial x_j} + \frac{\partial u_j}{\partial x_i}\right)\right] + \frac{\partial}{\partial x_j}\left(-\overline{\rho u_i' u_j'}\right) \tag{2}$$

where x_i (i = 1, 2, 3) represents the cartesian coordinates, ui are the corresponding velocity components, p is the pressure, ρ is the density, μ is the dynamic viscosity and $-\overline{\rho u_i' u_j'}$ are the Reynolds stresses.

For URANS model, additional transport equations for turbulence quantities are introduced. The additional transport equations required for turbulence closure are solved using the Shear Stress Transport (SST) k-ω model, which blends the k-ε and k-ω formulations. The SST model is chosen due to its ability to accurately predict turbulence effects in both the near-wall region and the freestream. The transport equations for the turbulent kinetic energy (k) and the specific turbulence dissipation rate (ω) are expressed as:

$$\frac{\partial(\rho k)}{\partial t} + \nabla \cdot (\rho U k) = \nabla \cdot \left[\left(\mu + \frac{\mu_t}{\sigma_k}\right)\nabla k\right] + P_k - \rho\beta^* k\omega \tag{3}$$

$$\frac{\partial(\rho\omega)}{\partial t} + \nabla \cdot (\rho U \omega) = \nabla \cdot \left[\left(\mu + \frac{\mu_t}{\sigma_\omega}\right)\nabla\omega\right] + \gamma\frac{P_k}{\nu_t} - \beta\rho\omega^2 + 2(1 - F_1)\frac{\rho\sigma_{\omega 2}}{\omega}\nabla k \cdot \nabla\omega \tag{4}$$

The production term for turbulent kinetic energy is given by $P_k = 2\mu_t S_{ij} S_{ij}$ where the strain rate tensor is defined as:

$$S_{ij} = \frac{1}{2}\left(\frac{\partial U_i}{\partial x_j} + \frac{\partial U_j}{\partial x_i}\right) \tag{5}$$

The turbulent eddy viscosity is computed as:

$$\mu_t = \frac{a_1 \rho k}{\max(a_1\omega, SF_2)} \tag{6}$$

where $S = \sqrt{2S_{ij}S_{ij}}$ is the mean strain rate magnitude. To account for wall effects and improve prediction in separated flows, the blending function F_1 is defined as:

$$F_1 = \tanh\left(\left(\min\left[\max\left(\frac{\sqrt{k}}{\beta^*\omega d}, \frac{500\nu}{d^2\omega}\right), \frac{4\rho\sigma_{\omega 2}k}{d^2}\right]\right)^4\right) \tag{7}$$

where d represents the distance to the closest wall. The SST formulation transitions smoothly

between k-ω near the wall and k-ε in the freestream by modifying the turbulent eddy viscosity and introducing a viscosity limiter. This limiter prevents overprediction of eddy viscosity in regions of strong flow separation.

The IDDES model was adopted for the present study due to its ability to accurately capture unsteady flow phenomena, such as vortex shedding and turbulent wake structures, while efficiently combining the features of RANS near the wall boundary region and LES in the unsteady separated regions (Liu et al., 2024). The IDDES model combines features of SST $k-\omega$ RANS model in the boundary layers with a LES in unseparated regions. The IDDES formulation of the SST $k-\omega$ model is achieved by modifying the dissipation term (Y_k) in the transport equation for k as shown in Eq. (9)

$$\frac{\partial(k)}{\partial t} + u_j \frac{\partial(k)}{\partial x_j} = \frac{\partial}{\partial x_j}\left[\left(\nu + \frac{\nu_t}{\sigma_k}\right)\frac{\partial k}{\partial x_j}\right] + G_k - Y_k \tag{8}$$

$$Y_k = \frac{k^{3/2}}{l_{\mathrm{RANS}}} \tag{9}$$

The L_{RANS} is the turbulent length scale for the RANS. However, in the IDDES, L_{RANS} length scale is replaced by L_{IDDES}, which is the IDDES turbulent length scale written below as:

$$L_{\mathrm{IDDES}} = f_d'(1 + f_e)L_{\mathrm{RANS}} + (1 - f_d')L_{\mathrm{LES}}) \tag{10}$$

Where f'_d is the blending function, f_e is an elevating function, L_{RANS} is the length scale for RANS and L_{LES} is for LES and is defined as:

$$L_{\mathrm{LES}} = C_{\mathrm{DES}}\Delta\,, L_{\mathrm{RANS}} = \frac{k^{1/2}}{\beta^*\omega} \tag{11}$$

Here $\beta^* = 0.09$ is a constant in the SST $k-\omega$, $\Delta = \min[\max\{C_w\Delta_{max}, C_{wd}, \Delta_{min}\}, \Delta_{max}]$ is the sub-grid length-scale between $\Delta_{min} = \min\{\Delta x, \Delta y, \Delta z\}$ and $\Delta_{max} = \max\{\Delta x, \Delta y, \Delta z\}$. C_w is the empirical constant, d is the nearest wall distance. The blending function is defined as $f'_d = \max\{1- f_{dt}), f_B\}$ where f_B is empirical blending function. When f_e is equal to zero, Eq. (10) can be written as:

$$L_{\mathrm{IDDES}} = L_{\mathrm{DDES}} = f_d' L_{\mathrm{RANS}} + (1 - f_d')L_{\mathrm{LES}} \tag{12}$$

Whereas, when f_e is higher than zero and f'_d is equal to f_B, Eq. (10) becomes:

$$L_{\mathrm{IDDES}} = L_{\mathrm{WMLES}} = f_B(1 + f_e)L_{\mathrm{RANS}} + (1 - f_B)L_{\mathrm{LES}} \tag{13}$$

Comprehensive explanations of the equations and coefficients can be found in Chen et al. (2022) Wang et al. (2024) and Siddiqui and Agelin-Chaab, (2023).

Test case, grid generation and boundary conditions

This study considered NREL 5MW baseline OWT blade (Jonkman, 2009). As discussed earlier in this paper, the windward blade tip section which comprises of NACA 64-618 airfoils were selected as the object of study due to their susceptibility to greater ice accumulation in offshore during cold climates. The blade tip airfoils considered spans from 44.55 m (r/R =

0.96)to 61.63m (r/R =1). Given the computational costs associated with simulating the full-scale geometry, a scaled model of the blade tip was chosen for analysis. This approach enables a detailed investigation of the flow characteristics around the blade using different turbulence models, while maintaining the fidelity needed to capture critical aerodynamic features relevant to the study. The scaled airfoil, with a chord length of c = 0.1 m was extruded along a span length of 0.5c to create a 3D blade. This extruded model is positioned at the center of the computational domain.

The domain extends 4c upstream from the blade leading edge, 12c downstream from the leading edge and spans 8c in the wall normal direction. This flow domain was used for the simulation to accurately capture wake development, vortex shedding and prevent flow reversal at the outlet. The domain was discretized using an unstructured mesh around the blade as illustrated in Fig. 1. As shown in the close-up view, the mesh maintains good orthogonality near the airfoil surface for accurate boundary layer resolution using prismatic inflation layers. To capture regions with high velocity gradients and strong shear forces on the wall of the airfoil, the first node was placed 0.0001 mm from the boundary ensuring a dimensionless wall distance (y^+) of less than 1. The growth ratio of the cells away from the wall was 1.2 times greater in size than the node before. To ensure grid adequacy, a grid independence study was conducted, and the final mesh consists of approximately 29M cells.

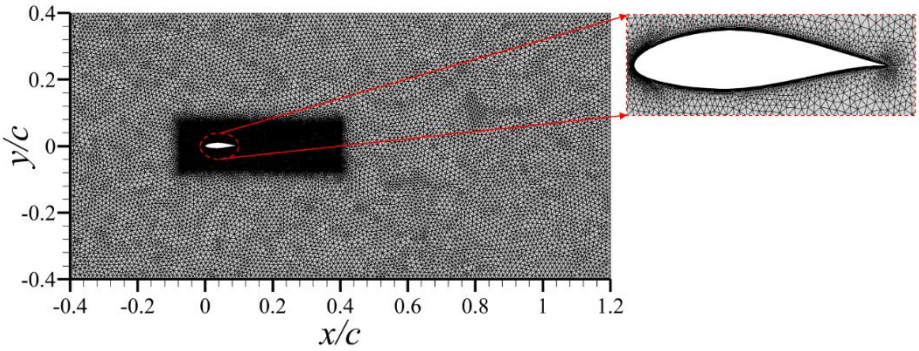

Figure 1: Grid distribution around the NACA 64-618 Blade.

Air at 15 °C with density of ρ_{air} = 1.225 kgm^{-3} and constant dynamic viscosity of μ_{air} = 1.789 × 10^{-5} Pa/s was used as a working fluid for the simulation. In terms of boundary conditions, a Dirichlet boundary condition prescribing a uniform velocity, U_e = 20 m/s was applied at the inlet, while a constant relative pressure of 0 Pa was imposed at the outlet. Free-slip conditions were also applied at the top, bottom and left-right side surfaces of the computational domain.

All numerical simulations were performed using ANSYS FLUENT 2024 R1. The simulations were conducted utilizing a second-order implicit temporal scheme to ensure enhanced accuracy in capturing time-dependent flow dynamics. Spatial terms discretization utilized a second-order upwind scheme to minimize numerical diffusion and improve the resolution of flow structures. Pressure-velocity coupling was performed by the SIMPLE algorithm ensuring robust convergence for the incompressible flow solver. The time step size was set to $\Delta t = 1 \times 10^{-5}$ s. To maintain numerical stability and accuracy, the maximum Courant-Friedrichs-Lewy (CFL= $u\Delta t/\Delta x$) number was constrained to 1 throughout the simulation. The convergence criterion for solving the momentum and continuity (Poisson) equations was defined as 1×10^{-6} based on the maximum residual difference in each velocity component. All the computations were performed using a high-performance computing cluster (Beluga) based on Intel Gold 6148 Skylake 2.4 GHz chip technology.

Validation

The URANS simulation was first validated using the experimental data byRomani et al. (2018). Figure 2 illustrates the variation of C_p along the normalized chord length (x/c) at $\alpha = -0.88°$. The numerical results from the present study show good agreement with experimental data across most of the chord length. However, a small discrepancy is observed in the suction region near the airfoil's upper surface ($x/c = 0.6$) where the numerical prediction slightly underestimates the experimental data with a relative error of approximately 15%.

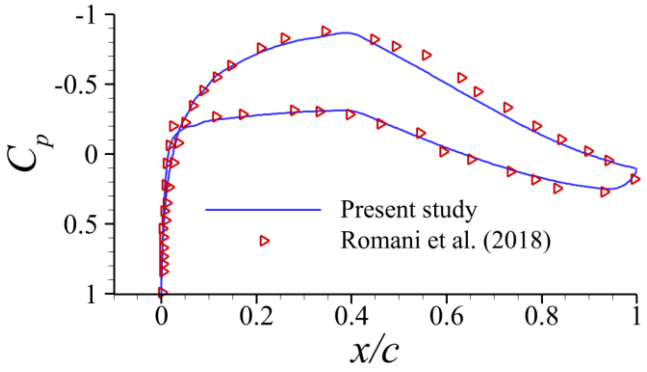

Figure 2: Comparison of pressure coefficient on the wall of the blade at $\alpha = -0.88°$ for experiment data and numerical study.

RESULTS AND DISCUSSIONS

Instantaneous flow fields

To gain a deeper understanding of the flow behavior around and downstream of the blade model, the normalized instantaneous streamwise velocity (U/U_e) is examined for both the URANS and DES models, as shown in Fig. 3 (a-b). The instantaneous streamwise velocity helps to visualize the transient flow features and provides insights into the unsteady nature of the flow around the blade. Generally, the flow topology revealed flow deceleration at the leading edge, acceleration at the suction surface of the blade and separation at the trailing edge due to adverse pressure gradient formed by the upstream flowing fluid. In both cases as shown in Fig.3 (a-b), a distinct reverse flow region ($U < 0$) is observed at the suction surface near trailing edge. For the URANS, the transient velocity fluctuations were not captured in the unsteady wake. Consequently, the flow structures around the blade appear less dynamic, and the streamwise velocity distribution is relatively smoother compared to the DES model. The instantaneous streamwise velocity in the DES model shows a much more intricate and dynamic flow field, with noticeable fluctuations and velocity gradients particularly at the trailing edge of the blade and the wake region. Also, the DES model captures the transient effects of vortex shedding, flow separation, and recirculation, which are critical in accurately representing turbulent, unsteady flows.

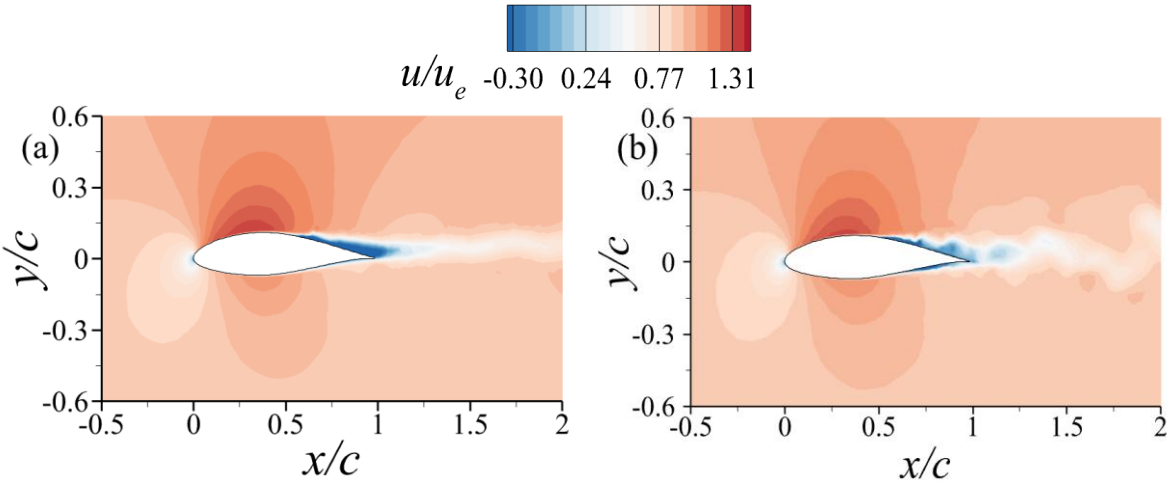

Figure 3: Instantaneous velocity contours for (a) URANS (b) DES at $\alpha = 12°$

The instantaneous spanwise vorticity, computed from $\omega_z = \left|\frac{\partial V}{\partial x} - \frac{\partial U}{\partial y}\right|$, are shown in Fig. 4(a-b) for both URANS and DES. The spanwise vorticity plots for both the URANS and DES simulations provide insightful comparisons regarding the flow characteristics around the blade. Notably, the flow topology reveals alternating vortex shedding from the upper and lower surfaces of the blade, flanked by regions of high vorticity magnitudes (red and blue). In Fig 4(a), there is clear evidence of a diffusive wake structure, which is as a result of the averaging nature of the turbulent fluctuations over time in the URANS model. This smooth, spread-out wake is characteristic of the URANS approach, which does not resolve fine-scale turbulent features but instead averages the turbulent effects, leading to a less detailed prediction of the wake dynamics.

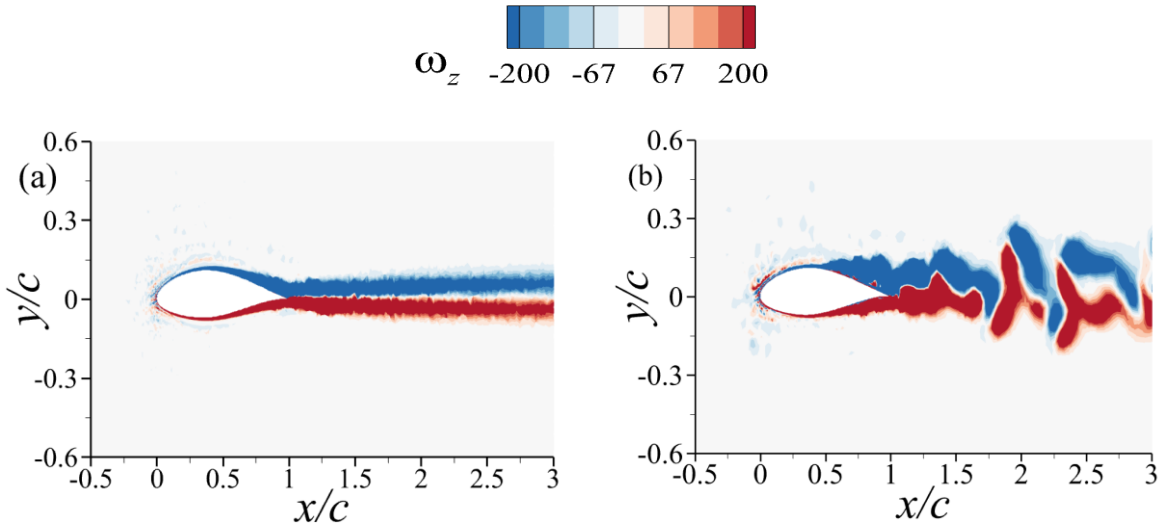

Figure 4: Spanwise vorticity contour around the airfoil for (a) URANS and (b) DES at $\alpha = 12°$

In Fig. 4(b), the DES simulation reveals a more detailed and structured wake. The localized high vorticity zones, particularly near the trailing edge, indicate the presence of large-scale eddies and vortex shedding that the DES model is capable of resolving. This vortex shedding arises from the shear layer instabilities at the interface, comparable to the Kelvin-Helmholtz (KH) type instabilities. The KH instabilities at the interface amplify small perturbations, which

then grow and roll up into vortices, creating wave-like structures similar to the von Kármán vortex street. As compared to the URANS model, these instabilities are more accurately captured. This enhanced wake structure observed in the DES model provides a much clearer representation of the turbulent dynamics, which is a direct consequence of the model's hybrid approach.

To gain an intuitive insight into the vortical structures generated around and downstream of the blade model, three dimensional iso-surfaces of the Q-criterion, defined as $Q = \frac{1}{2}\left(\overline{\Omega_{ij}}\,\overline{\Omega_{ij}} - \overline{S_{ij}}\,\overline{S_{ij}}\right)$ where $\overline{\Omega_{ij}}$ is the vorticity rate tensor and $\overline{S_{ij}}$ is the strain rate tensor is used. Based on the definition, vortical structures exist when $Q > 0$, reflecting the local dominance of vorticity than strain. The threshold for the normalized Q-criterion ($Q^* = Q(\frac{c}{u_e})^2$) values used for the visualization is $Q^* = 5$. Figure 5 (a-b) shows the vortex structures obtained using the URANS and DES model respectively. It is interesting to note that the vortex structures around blade are shown to be less densely packed and show fewer fine scale structures in the URANS model, as it primarily resolves time-averaged quantities. On the other hand, the DES model captures a much denser distribution of vortices characterized by hairpin and roll-up vortices compared to URANS. Also, the URANS model was unable to predict flow separation at the trailing edge of the blade as the DES model clearly predicted the separation highlighting its ability to better resolve complex flow phenomena in detached areas.

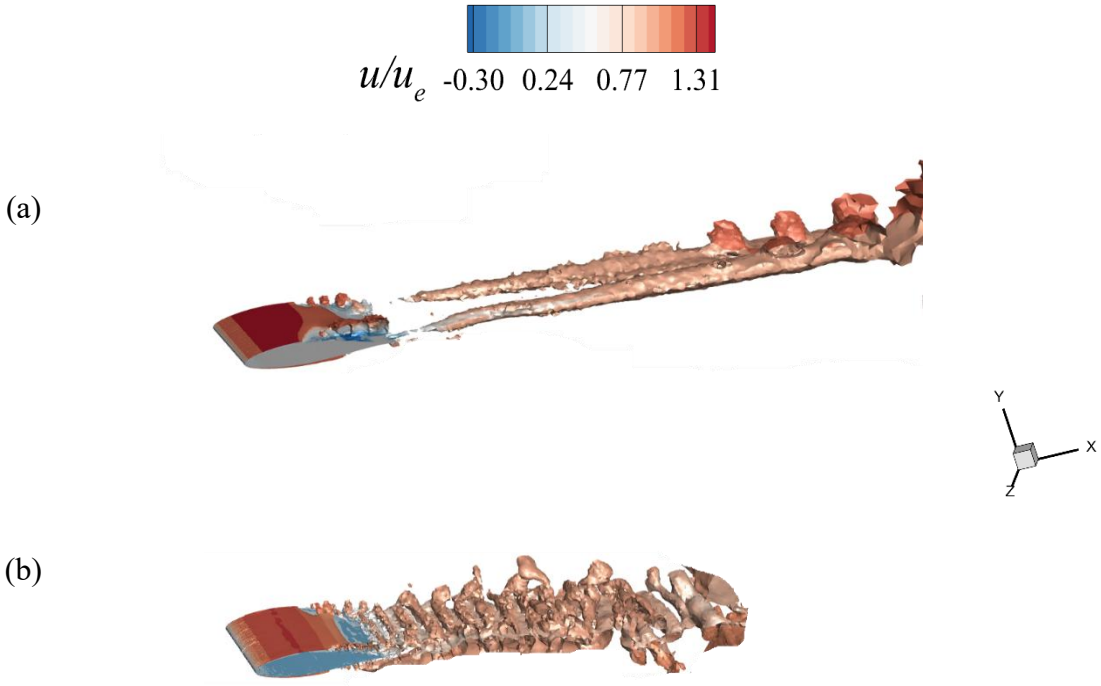

Figure 5: Vortex structures at $Q^* = 5$ (colored with U/U_e) around the blade model and in the wake region for (a) URANS (b) DES

CONCLUSIONS

In this study, the performance of two turbulence models, URANS and DES were compared for simulating the flow around the tip section of the NREL 5MW OWT blade at a higher angle of attack (α = 12°). The results demonstrated that while URANS provides good predictions for attached flows, it significantly underpredicts separated flows and lacks the

ability to resolve key unsteady phenomena, particularly in the wake region. In contrast, the DES model, by resolving large eddies and capturing flow separation more accurately, offers a much better representation of vortex shedding, recirculation regions, and turbulent dynamics. The enhanced accuracy of DES in predicting the flow separation at the trailing edge further emphasizes its superiority over URANS for modeling complex unsteady flows in offshore wind turbine applications.

ACKNOWLEDGEMENTS

The authors acknowledge financial support from National Sciences and Engineering Research Council of Canada Discovery grant (RGPIN-2024-04606) awarded to BN-K and the support of Digital Research Alliance of Canada

REFERENCES

Abbott, I. H., & Von Doenhoff, A. E. (2012). *Theory of wing sections: including a summary of airfoil data*. Courier Corporation.

Argyropoulos, C. D., & Markatos, N. C. (2015). Recent advances on the numerical modelling of turbulent flows. *Applied Mathematical Modelling, 39*(2), 693-732.

Bangga, G., Kusumadewi, T., Hutomo, G., Sabila, A., Syawitri, T., Setiadi, H., ... & Kristiadi, S. (2018a). Improving a two-equation eddy-viscosity turbulence model to predict the aerodynamic performance of thick wind turbine airfoils. *Journal of Physics: Conference Series, 974*(1).

Bangga, G., Weihing, P., Lutz, T., & Krämer, E. (2018b). Hybrid RANS/LES simulations of the three-dimensional flow at the root region of a 10 MW wind turbine rotor. In *New Results in Numerical and Experimental Fluid Mechanics XI: Contributions to the 20th STAB/DGLR Symposium Braunschweig, Germany, 2016* (pp. 707-716).

Chakraborty, P., Balachandar, S., & Adrian, R. J. (2005). On the relationships between local vortex identification schemes. *Journal of Fluid Mechanics, 535*, 189-214.

Chen, G., Li, X.-B., & Liang, X.-F. (2022). IDDES simulation of the performance and wake dynamics of the wind turbines under different turbulent inflow conditions. *Energy, 238*, 121772.

Garnier, E., Adams, N., & Sagaut, P. (2009). *Large Eddy Simulation for Compressible Flows*. Springer.

Hasheminasab, S. M., Karimian, S. M. H., Noori, S., Saeedi, M., & Morton, C. (2021). Experimental investigation of the wake dynamics for a NACA0012 airfoil with a cut-in serrated trailing-edge. *Physics of Fluids*, *33*(5).

Jeong, J., & Hussain, F. (1995). On the identification of a vortex. *Journal of Fluid Mechanics, 285*, 69-94.

Jonkman, J. (2009). Definition of a 5-MW Reference Wind Turbine for Offshore System Development. *National Renewable Energy Laboratory*.

Kato, M., & Nagano, Y. (1993). Formation mechanism of longitudinal vortices in turbulent boundary layers. *Physics of Fluids A: Fluid Dynamics, 5*(11), 2921-2931.

Lee, C., & Sung, H. J. (2001). Characteristics of wall pressure fluctuations in separated and reattaching flows. *Journal of Fluid Mechanics, 437*, 41-72.

Liu, B., Yan, X., Ouyang, W., & Vanierschot, M. (2024). Comparison study of the vortical structures in the wake of a rim-driven thruster and a ducted propeller in bollard conditions. *Ocean Engineering, 306*, 118064.

Menter, F. R. (1994). Two-equation eddy-viscosity turbulence models for engineering applications. *AIAA Journal, 32*(8), 1598-1605.

Mittal, R., & Moin, P. (1997). Suitability of upwind-biased schemes for large-eddy simulation of turbulent flows. *AIAA Journal, 35*(8), 1415-1417.

Quayson-Sackey, E., Nyantekyi-Kwakye, B., & Ayetor, G. K. (2024). Technological advancements for anti-icing and de-icing offshore wind turbine blades. *Cold Regions Science and Technology*, 104400.

Rumsey, C. L., & Gatski, T. B. (2001). Recent turbulence model advances applied to aerodynamic flows. *Journal of Aircraft, 38*(5), 829-835.

Shur, M. L., Spalart, P. R., Strelets, M. K., & Travin, A. K. (2008). A hybrid RANS-LES approach with delayed-DES and wall-modeled LES capabilities. *International Journal of Heat and Fluid Flow, 29*(6), 1638-1649.

Siddiqui, N. A., & Agelin-Chaab, M. (2023). Investigation of the wake flow around the elliptical Ahmed body using detached Eddy simulation. *International Journal of Heat and Fluid Flow, 101*, 109125.

Spalart, P. R. (2000). Strategies for turbulence modelling and simulations. *International Journal of Heat and Fluid Flow, 21*(3), 252-263.

Spalart, P. R., Jou, W. H., Strelets, M., & Allmaras, S. R. (1997). Comments on the feasibility of LES for wings, and on a hybrid RANS/LES approach. *Advances in DNS/LES, 1*(1), 137-147.

Strelets, M. (2001). Detached eddy simulation of massively separated flows. *AIAA Journal, 39*(11), 2006-2013.

Wang, Z., Wu, T., Wang, L., Cao, W., & Luo, W. (2024). Near-field wake dynamics of propellers affected by double-sided barnacles attachment. *Physics of Fluids, 36*(10).

Wang, M., Freund, J. B., & Lele, S. K. (2014). Computational prediction of flow-generated sound. *Annual Review of Fluid Mechanics, 36*(1), 483-505.

Xiao, M. J., & She, Z. S. (2020). Precise drag prediction of airfoil flows by a new algebraic model. *Acta Mechanica Sinica, 36*(1), 35-43.

Zhong, B., Scheurich, F., Titarev, V., & Drikakis, D. (2009). Turbulent flow simulations around a multi-element airfoil using URANS, DES, and ILES approaches. In *19th AIAA Computational Fluid Dynamics, 22-25 June 2009, San Antonio, Texas, USA* (p. 3799).